

Polarized X-ray absorption spectroscopy of the low-temperature photoproduct of carbonmonoxy-myoglobin

Stefano Della Longa,^{a,b*} Alessandro Arcovito,^c Beatrice Vallone,^c Agostina Congiu Castellano,^{b,d} Richard Kahn,^e Jean Vicat,^e Yvonne Soldo^f and Jean Louis Hazemann^f

^aDipartimento di Medicina Sperimentale, Università L'Aquila, 67100 L'Aquila, Italy, ^bINFM, Università 'La Sapienza', 00185 Roma, Italy, ^cDipartimento di Scienze Biochimiche, Università 'La Sapienza', 00185 Roma, Italy, ^dDipartimento di Fisica, Università 'La Sapienza', 00185, Roma, Italy, ^eInstitute de Biologie Structurale, 41 Rue de Martyrs, 38027 Grenoble, France, and ^fLaboratoire Crystallographie, CNRS, 25 Avenue de Martyrs, F-38043 Grenoble, France. E-mail: dellalonga@vaxaq.cc.univaq.it

(Received 3 May 1999; accepted 10 August 1999)

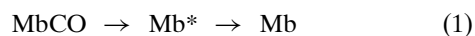
Visible light can break the Fe—CO bond in Fe(II) carbonmonoxy-myoglobin (MbCO) giving an unligated product (Mb*) that is almost stable at $T < 30$ K. Fe *K*-edge polarized X-ray absorption spectra (P-XAS) of the photoproduct ($T = 20$ K) of an oriented single crystal ($0.2 \times 0.2 \times 0.3$ mm) of sperm whale MbCO (space group $P2_1$) have been collected. By rotating the crystal the X-ray photon polarization vector has been oriented almost parallel (with an angle $\alpha = 23^\circ$) or perpendicular ($\alpha = 86^\circ$) to the heme normal of each myoglobin molecule. The crystal was continuously illuminated by a white-light source during the data collection. The polarized data give novel information on the heme electronic/structural rearrangement following photolysis. The XANES (X-ray absorption near-edge structure) spectrum polarized in the direction close to the Fe—CO bond changes dramatically after photolysis, exhibiting a shift of ~ 2 eV, due to electronic relaxation of empty states of p_z symmetry, while more subtle changes are observed in the spectrum polarized along the heme plane, sensitive to the heme-plane geometry. Changes in the pre-edge region can be interpreted to provide insight into the electronic structure of the highest occupied and lowest unoccupied molecular orbitals (HOMO—LUMO) in the MbCO \rightarrow Mb* photochemical reaction at low temperature.

Keywords: hemoproteins; XANES; photolysis.

1. Introduction

Visible light can be used in the laboratory to induce photolysis of carbonmonoxy-myoglobin (MbCO), *i.e.* to trigger the dissociation of the CO molecule from the Fe-heme complex in the hydrophobic core of myoglobin (Mb). This protein dynamic event has been addressed by many theoretical (Case & Karplus, 1979; Sassaroli & Rousseau, 1986; Elber & Karplus, 1987; Vitkup *et al.*, 1997) and experimental (Austin *et al.*, 1975; Alben *et al.*, 1980; Kuriyan *et al.*, 1986; Powers *et al.*, 1987; Phillips, 1990; Steinbach *et al.*, 1991; Quillin *et al.*, 1993; Lim *et al.*, 1997) studies.

The dissociation process is represented in a simplified scheme by the three-well model



in which MbCO is the starting main state of the protein, Mb is the final main state when the CO molecule is in the solvent, and Mb* represent all the intermediate states when the CO molecule is in the protein matrix. The crystal structures of MbCO and Mb at a resolution of 1.15 Å

(Kachalova *et al.*, 1999) show that CO dissociation at room temperature is accompanied by concerted motions of the iron, the heme and helices *E* and *F*. Multiple time-dependent energy barriers affect the motion of the CO molecule within the protein matrix, resulting in non-exponential time dependence and non-Arrhenius temperature dependence of the binding kinetics. At room temperature the photo-dissociated CO molecule rebinds to the iron on the microsecond time scale, so that fast detection techniques have to be applied to reveal intermediate states before recombination (Franzen *et al.*, 1995; Srajer *et al.*, 1996). At $T < 160$ K the CO recombination is still fast but limited within the closed heme pocket (geminate recombination) (Scott & Gibson, 1997). At $T < 30$ K the CO rebinds very slowly (Iizuka *et al.*, 1974), by molecular tunnelling (Alben *et al.*, 1980), so that almost a 100% conversion to the photoproduct can be achieved in the experimental time window of standard techniques, but the protein matrix remains frozen in the conformation of ligated MbCO.

X-ray diffraction studies of the cryogenic metastable Mb* photoproduct of MbCO at $T = 20$ K (Schlichting *et al.*,

1994) and $T = 40$ K (Teng *et al.*, 1987) reported different positions of the CO molecule in the heme pocket. According to a later X-ray study (Teng *et al.*, 1997) it has been proposed that the different positions found correspond to migration of the CO molecule. At the same time the relaxation of the unligated Fe-heme towards the structure of Mb is hindered by protein restraints at such a low temperature, while at room temperature the relaxation is almost complete (Franzen *et al.*, 1995; Srajer *et al.*, 1996), so that low-temperature studies seem relevant to identify the restrained parameters of the Fe-heme, directly linked to protein motions. The X-ray data are partially in disagreement concerning the extent of relaxation at low temperature: either about 70% according to Schlichting *et al.* (1994) (the Fe atom moves out of the heme plane by 0.2 \AA at $T = 20$ K, under continuous illumination by a white-light source), or about 30% according to Teng *et al.* (1997) (the Fe atom moves out of the heme plane by only 0.1 \AA at $T = 40$ K, after a short laser illumination at 633 nm, and does not relax further after prolonged illumination). These discrepancies are hard to explain as they only differ in the photolysis protocols.

A spectroscopic probe, the near-IR band III at 760 nm, is believed to be sensitive to the five-coordinated structure of Fe-heme, and to the Fe-heme relaxation processes (Iizuka *et al.*, 1974). It has been assigned to a porphyrin (a_{2u}) \rightarrow Fe(d_{yz}) charge transfer transition. It is found at different energy positions for Mb (758 nm) and Mb* (772 nm) between 4.2 and 40 K. By increasing the temperature after photolysis of MbCO at 10 K, the Mb* band exhibits kinetic hole burning (*i.e.* a shift of the band following partial ligand rebinding) between 50 and 120 K, stays fairly constant between 120 and 150 K, and shifts towards the value of Mb above 150 K. This last shift has been taken as evidence of thermally induced Mb* \rightarrow Mb relaxation. More recently, a light-induced Mb* \rightarrow Mb relaxation has been reported (Nienhaus *et al.*, 1994), probed by a shift of the frequency of this band in Mb* after extended illumination. As suggested by the observed time and temperature dependence of the Soret and Band III shifts in horse myoglobin, relaxation dynamics at the heme occurs on a time scale of nanoseconds, considerably faster than geminate rebinding; however, a correlation has been found between the heme relaxation rates and geminate rebinding rates measured on different mutants, showing a connection between the relaxation process and the protein function (Lambright *et al.*, 1991; Franzen & Boxer, 1997).

X-ray absorption spectroscopy (XAS) probes photoelectron transitions from a deep metal core level to final unoccupied continuum states with selected symmetry formed by interference between the outgoing photoelectron wave from the metal centre and the backscattering waves from neighbouring atoms (Pin *et al.*, 1994). By the EXAFS (extended X-ray absorption fine structure) spectra one can measure, in principle, distances between the metal centre and backscattering atoms with a 0.02 \AA precision, giving insight into the structure and dynamics of heme-

proteins in solution, and being suitable for studying geminate recombination at low temperature. Unfortunately the EXAFS results reported so far on the low-temperature photoproduct of MbCO in solution are controversial. By the extracted first-shell filtered data, measuring the variation of the average distance Fe– N_p , a different degree of Fe-heme relaxation has been outlined by various EXAFS studies: in sperm whale MbCO in solution after photolysis at $T = 10$ K (Chance *et al.*, 1983; Powers *et al.*, 1984) the values of $d(\text{Fe}–N_p) = 2.01 \pm 0.02 \text{ \AA}$ in MbCO and $d(\text{Fe}–N_p) = 2.03 \pm 0.02 \text{ \AA}$ in Mb*CO were measured; another EXAFS work (Teng *et al.*, 1987) reported a distance $d(\text{Fe}–N_p) = 1.98 \pm 0.02 \text{ \AA}$ in an MbCO dried film sample, without variations from this distance after photolysis at $T = 5$ K. More recently, a different kind of analysis [global mapping of structural solution, by Chance *et al.* (1995)] was used to fit the full EXAFS spectrum of the photoproduct at 10 K of horse MbCO (pH 9) after 5 min of illumination by a high-intensity white-light source. Evaluation of these data placed the Fe– N_p average distance close to the value found for Mb, in which $d(\text{Fe}–N_p) = 2.06 \text{ \AA}$. Apart from factors due to the different protocols and sample conditions used in the EXAFS experiments, it is possible that some error was due to intrinsic limitations of the technique when applied in solution to determine the coordination number of the Fe atom, and to solve the iron first-shell distances, convoluted in the first Fourier peak. For example, previous EXAFS works (Teng *et al.*, 1987) made use of the method of Eisenberger *et al.* (1978) to deconvolute the mixed first Fe coordination shell in MbCO and Mb*, making use, for any atomic distance, of the same value of the threshold energy E_0 through which the electron wavenumber k was calculated from the X-ray energy. The solution was searched by varying E_0 over a reasonable range. However, by looking, for example, at the polarized XANES spectra of Mb* in §3, a shift of 2 eV should be applied to E_0 between the $\varepsilon // c$ spectra, that probe essentially $d(\text{Fe}–N_p)$, and the $\varepsilon // a^*$ spectra, that probe $d(\text{Fe}–N_e)$, so that different values for the atomic distances could be expected.

Spectroscopic evidence of partial heme relaxation in sperm whale Mb* is obtained by looking at the XANES (X-ray absorption near-edge structure) region. The absorption threshold of the spectrum of Mb is redshifted relative to that of MbCO by about 2.5 eV while the spectrum of Mb* (at $T < 20$ K) is redshifted with respect to MbCO by about 1 eV (Teng *et al.*, 1987; Della Longa *et al.*, 1994). The absorbing Fe atom in both Mb* and Mb is five-coordinated, and has the same oxidation state and spin state; in such conditions a redshift of a threshold going from Mb* to Mb was explained, according to the Natoli rule (Natoli, 1983), by a lengthening of the first-shell distances (Della Longa *et al.*, 1994). Moreover, a relation between the Fe-heme displacement and the XANES features has been proposed (Chance *et al.*, 1986; Miller & Chance, 1995) by looking at the ligand field indicator region (LFIR) (7150–7250 eV) that attributed changes in this region to focusing effects between the Fe absorbing atom and the

backscattering pyrrolic rings of the porphyrin, leading to an empirical formula correlating the LFIR ratio between two peaks of this region and the Fe displacement: LFIR ratio = $(2.3 \text{ \AA}^{-1} \times \text{Fe displacement}) + 0.66$.

The possibility of a P-XAS investigation on a small protein crystal of opportune symmetry, at very low temperature, adds original structural information on the Fe-heme site of the MbCO photoproduct at low temperature. The use of both X-ray dynamic focusing onto the $0.2 \times 0.2 \text{ mm}$ size of the MbCO crystal, and a high-energy-resolving 24-element array fluorescence detector, has allowed the collection of polarized XANES spectra, and preliminary polarized EXAFS spectra in the range $k = 2\text{--}13 \text{ \AA}^{-1}$. Orienting the X-ray polarization vector either along the Fe—CO bond or along the heme plane has made it possible to distinguish changes of axial and planar parameters of the Fe coordination sphere, and to re-interpret previous XANES experiments in solution. Only XANES results are discussed in the present paper. However, solving quantitatively these first shell parameters by polarized EXAFS should be easier than by EXAFS in solution. The *parallel* XAS investigation of heme proteins single crystals and solution samples can be greatly helpful to support X-ray diffraction and other spectroscopic data on this outstanding protein dynamics problem.

2. Materials and methods

2.1. Crystal preparation

Monoclinic ($P2_1$) single crystals of native sperm whale myoglobin purchased before the ban were soaked for 8 h in a thoroughly degassed and CO-saturated solution containing mother liquor (3.25 M ammonium sulfate with 0.05 M phosphate buffer, pH 6.5) and 8 mg ml^{-1} Na-dithionite. Distinct colour changes accompanied the formation of Mb from met-Mb and MbCO from Mb. Immediately before starting the experimental protocol a crystal was suspended in a cryoprotectant solution containing the same components and 20% glycerol, and put in a quartz capillary in anaerobic conditions.

2.2. Crystal orientation and cryogenics

The quartz capillary containing the crystal was mounted on a goniometric head and pre-oriented on a FAST diffractometer at the Institute de Biologie Structurale (IBS), close to the EXAFS beamline. The *b*-axis of the monoclinic cell was oriented parallel to the axis of the goniometric head. The position of the *a*-axis was marked and the goniometric head was rapidly frozen in an open-cycle helium cryostat previously lowered to 80 K. The temperature of the crystal holder was monitored by two platinum/carbon resistors. It was lowered below 200 K in less than 1 min. Other MbCO crystals were subjected to the same protocol (except freezing) to check for damaging effects of the cryoprotectant along with the time spent before lowering at low temperature. The quality of crystal diffraction was found not to decay appreciably within the

first 24 h, which greatly exceeds the time required for our experimental protocol before freezing.

A pictorial view of the crystal unit cell of myoglobin, including the Fe-heme sites (with proximal histidine and the CO ligand) of the two symmetry-related myoglobin molecules, is represented in Fig. 1(a). The unit cell is seen along a projection parallel to the *b*-axis. The *b*-axis was oriented parallel to the rotation axis of the sample holder of the cryostat and each angular position around the *b*-axis was reached by a step motor having a formal accuracy of 0.01° . However, the real error depends on the accuracy by which the initial direction of the *a*-axis was marked, evaluated as $\pm 2^\circ$.

2.3. Photolysis protocol

Polarized XAS spectra of the MbCO crystal were acquired at $T = 100 \text{ K}$ by rotating the sample around the *b*-axis, *i.e.* by changing the orientation of the polarization X-ray vector ε from the $\varepsilon // c$ orientation to the $\varepsilon // a$ orientation. Then the crystal was cooled at $T = 20 \text{ K}$ (see Table 1) and photolysis was achieved using white light from a fibre-optic illuminator for about 3 h. A UV/V microspectrophotometer was not available at the beam station,

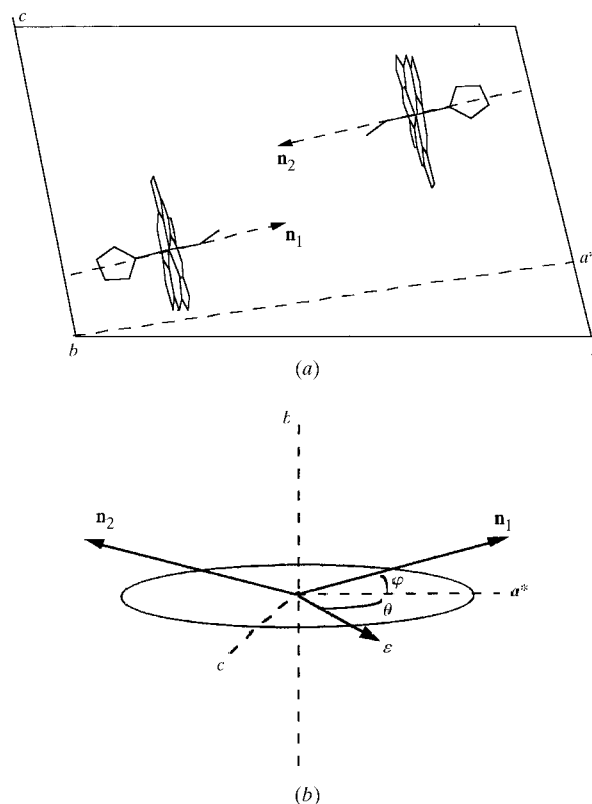


Figure 1
(a) Pictorial view of the arrangement of the two Fe-heme sites (including the proximal histidine imidazole and the CO ligand) in the unit cell of an MbCO single crystal. The view is projected along the *b* axis of the monoclinic crystal. (b) Geometry of the heme normals and the photon polarization vector, applied on the same origin, in the orthogonal crystal system a^*bc .

Table 1
Photolysis protocol.

Crystal	MbCO, $P2_1$, $0.2 \times 0.2 \times 0.3$ mm
Cooling	Cryostat liquid-He open flow at final temperature of 20 K
Rapid freezing	Cold He gas
Light source	White light from fibre-optic illuminator with integrated power density between 500 and 600 nm of 5×10^{-2} mW mm ⁻²
Photolysis protocol	Continuous. X-ray exposure after 3.5 h of illumination
Total illumination time	~500 min
Photolysis rate	0.001–0.1 s ⁻¹
Collection statistic	Fluorescence, using 24-element Ge detector. 30–1000 X-ray counts s ⁻¹ per element, <i>i.e.</i> 3000–100 000 counts per energy point. N/S = 3×10^{-3}
Collection time	~30–40 min per spectrum

so we have only indirect indications that the crystal was fully photolysed (>95%). These are as follows.

(i) At $T = 20$ K the steady state in photolysis kinetics corresponds to almost 100% of photolysis.

(ii) The calculated optical density (OD) of our crystal changes from OD = 192 at 420 nm to OD = 14 at 540 nm, and to OD = 0.1 at 630 nm, so that efficient photolysis on the sample is induced by photons between 500 and 600 nm. The sample was maintained under illumination for the duration of the experiment, like the protocol of Schlichting *et al.* (1994). Before collecting P-XAS spectra, distinct spectral changes in the $\varepsilon // a$ XANES spectra at $E = 7124$ eV were monitored until a steady state was reached. The kinetic curve of the X-ray absorption difference $[I_{7124}(t) - I(0)]/[I_{7124}(\infty) - I(0)]$ reached saturation in less than 1 h with an integrated irradiation power density (between 500 and 600 nm) of 5×10^{-2} mW mm⁻². The same saturation limit $I_{7124}(\infty)$ at $T = 20$ K was obtained by changing the intensity of irradiation.

2.4. Polarized XANES of myoglobin

With a structure that has a symmetry axis (symmetry C_4 , approximately that of the Fe-heme site) it is advantageous to calculate the XAS components linearly polarized along the symmetry axis (the heme normal), I_{normal} , and along a direction in the C_4 plane (the heme plane), I_{heme} . Assuming perfect C_4 symmetry, for a certain angle α between the polarization vector ε and the heme normal of one myoglobin molecule, the polarized spectrum I_α is given, as a function of I_{heme} and I_{normal} , simply by

$$I_\alpha = I_{\text{normal}} \cos^2 \alpha + I_{\text{heme}} (1 - \cos^2 \alpha), \quad (2)$$

and for the two myoglobin molecules oriented with angles α_1 and α_2 it will be equal to the sum $I_{\alpha_1} + I_{\alpha_2}$.

A useful geometry to describe the polarized absorption experiment in the case of the MbCO crystal is shown in Fig. 1(b), in the a^*bc orthogonal coordinate system of the crystal. In this system, to rotate the crystal around the b axis is equivalent to rotating the ε vector in the a^*c plane. θ is

the angle between the vector ε and the axis a^* , taken as the reference axis, and φ is the angle between both the heme normals and axis a^* . The two heme planes lie approximately in the bc plane (as seen in Fig. 1a), while the two heme normal vectors \mathbf{n}_1 and \mathbf{n}_2 lie approximately in the a^*b plane. By rotating the ε vector on the a^*c plane by an angle θ , one has

$$\cos \alpha_1 = \cos(\varepsilon \mathbf{n}_1) = \cos \theta \cos \varphi = -\cos \alpha_2, \quad (3)$$

hence the contributions I_{α_1} and I_{α_2} are equivalent for any value of θ , and the measured XAS spectrum at an angle θ with respect to the a^* axis as a function of I_{heme} and I_{normal} is

$$I_\theta = I_{\text{normal}} \cos^2 \theta \cos^2 \varphi + I_{\text{heme}} (1 - \cos^2 \theta \cos^2 \varphi). \quad (4)$$

The angle φ is equal to 23° in our crystal; therefore one obtains as extreme limits for polarization measurements with our MbCO crystal,

$$I_{\theta=0} = I_{\varepsilon//a^*} = 0.85 I_{\text{normal}} + 0.15 I_{\text{heme}}, \quad (5)$$

$$I_{\theta=90} = I_{\varepsilon//c} = 0.005 I_{\text{normal}} + 0.995 I_{\text{heme}}. \quad (6)$$

2.5. XAS measurement

X-ray absorption spectra have been collected at the CRG-IF BM32 beamline of ESRF, Grenoble (France), in the 2/3 filling mode, 150 mA. The monochromator at this beamline is an Si(111) double crystal, in which the second crystal is elastically bent to a cylindrical cross section. The X-ray photon beam was vertically focused by an Ni–Pt mirror, and dynamically sagittally focused in the horizontal size onto the 0.2×0.2 mm² spot of the MbCO crystal distant 42 m from the source. A high-energy-resolving 24-element array detector from EG&G Industries allowed the collection of XAS in fluorescence mode. The number of fluorescence counts changed from ~30 counts s⁻¹ per element (before the Fe K -edge) to ~1000 counts s⁻¹ per element (after the edge), so that 3000–100 000 counts per energy point were obtained with a total collection time of 30–40 min for each spectrum. With such a photon statistic, polarized XANES spectra and preliminary EXAFS spectra (these latter not presented here) were acquired in the range $k = 2.5$ – 13 \AA^{-1} .

3. Results

The $\varepsilon // a^*$ (solid curve) and the $\varepsilon // c$ (dotted curve) polarized XANES spectra of an MbCO single crystal at $T = 100$ K are shown in Fig. 2. These spectra are quite similar to those reported at room temperature by Bianconi *et al.* (1985), showing that our cryogenic protocol did not damage the MbCO crystal, and ruling out the presence of a relevant percentage of met-Mb in the crystal. As stated in §2 [equations (5) and (6)], the $\varepsilon // c$ spectrum contains a 99.5% contribution from scattering pathways within the heme

plane, while the $\varepsilon // a^*$ spectrum contains a 15% contribution from scattering pathways within the heme plane and an 85% contribution from scattering pathways along the heme normal.

In the pre-edge region, two peaks P_1 and P_2 are distinguishable [although using X-ray focusing optics with the Si(111) crystal limits the energy resolution], peak P_1 being polarized along the heme normal and peak P_2 being polarized on the heme plane. A small percentage of peak P_2 also appears in the $\varepsilon // a^*$ spectrum. Peak P_1 is assigned to a partially allowed (in an approximately C_{4v} symmetry) dipole transition from the core state $1s$ to an empty molecular orbital with z^2 symmetry, including the perturbed $Fe(d_{z^2})$ orbital. Peak P_2 has been assigned to a partially allowed dipole transition to degenerate antibonding molecular orbitals formed by mixing the $CO(\pi^*)$ MO and the $Fe(d_{xz}, d_{yz})$ atomic orbitals (Cartier *et al.*, 1992). Peaks in the continuum (A , C , D and C_2) are assigned to multiple-scattering resonances due to interference between the photoelectron wave created at the absorbing Fe site and the waves scattered from neighbouring atomic potentials. The strong peaks C and C_2 are completely $\varepsilon // a^*$ polarized and are predicted by the XANES theory to be due to focused scattering on the Fe—C—O and Fe—His photoelectron pathways (Bianconi *et al.*, 1985) so they are highly sensitive to the Fe—C—O geometry (Fe—C distance and Fe—C—O tilting/bending angle); peak D and shoulder A are $\varepsilon // c$ polarized due to scattering on the heme plane; their intensity should depend on heme doming effects in the dissociation process.

The $\varepsilon // a^*$ polarized XAS spectra of MbCO (dotted curve) and its photoproduct Mb* (solid curve) at $T = 20$ K are reported in Fig. 3(a). Photolysis has dramatic effects on this spectrum polarized near the heme normal. After breaking the Fe—CO bond a completely new spectrum appears with different values of edge position, and

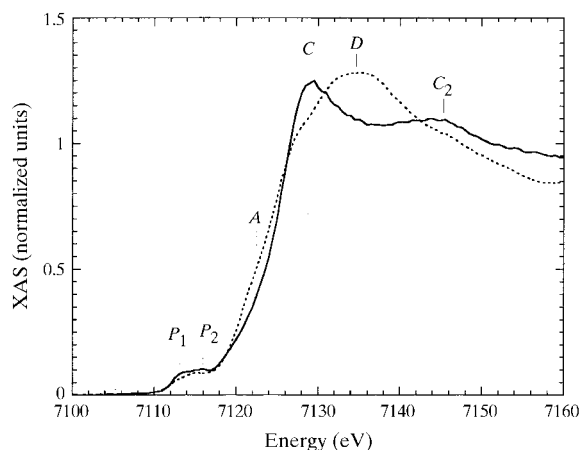


Figure 2
 $\varepsilon // a^*$ (solid line) and $\varepsilon // c$ (dotted line) polarized XANES spectra of MbCO at $T = 100$ K. Pre-edge peaks probe transitions to the LUMO orbitals of the Fe-heme system. Peaks C and C_2 are due to focused axial scattering including the imidazole histidine and the CO ligand. Peaks A and D probe heme plane distortions.

prominent features. The $\varepsilon // c$ polarized XAS spectra of MbCO and Mb* are shown in Fig. 3(b). The effects of photolysis on this spectrum, sensitive to the heme geometry, are much more limited in the XANES region; however, in the EXAFS region the maxima at about 7200 and 7270 eV are redshifted in Mb*, suggesting a change in the frequency of the main oscillating component of the EXAFS signal, in agreement with the expected partial elongation of $d(Fe-N_p)$.

The $\varepsilon // a^*$ and $\varepsilon // c$ polarized XANES spectra of MbCO (dotted curves) and Mb* (solid curves) are shown in Figs. 4(a) and 4(b). In the $\varepsilon // a^*$ polarization the absorption edge of Mb* is redshifted by about 2.5 eV and one observes the disappearance of the C and C_2 peaks, and the appearance of new features B_0 (the shoulder at ~ 7120 eV), B at ~ 7126 eV, B_2 at ~ 7132 eV and B_3 at ~ 7144 eV. The intensity of peak P_1 assigned to a $1s \rightarrow 3d_{z^2}$ transition lowers a little.

The $\varepsilon // c$ XANES polarized spectra of MbCO and Mb* are shown in Fig. 4(b) in the same way as in Fig. 4(a). A very small energy shift (if any) of the absorption threshold (<0.5 eV) is measured. The pre-edge peak P_2 in MbCO,

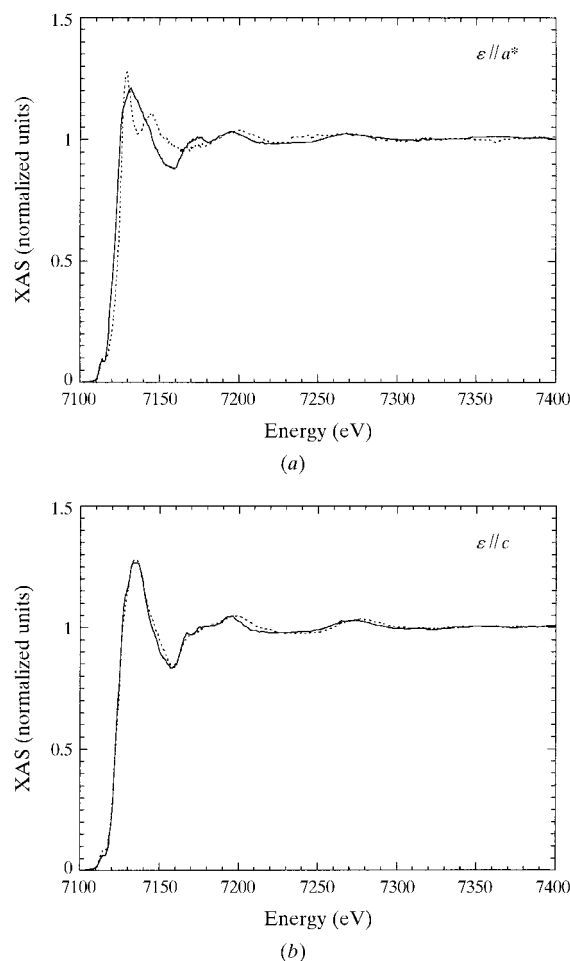


Figure 3
(a) $\varepsilon // a^*$ polarized XAS spectra of MbCO (dotted curve) and its photoproduct Mb* at $T = 20$ K (solid curve). (b) $\varepsilon // c$ polarized XAS spectra of the same samples.

assigned to $1s \rightarrow \text{CO}(\pi^*) \text{MO} + \text{Fe}(d_{xz}, d_{yz})$ transition, decreases in intensity. A small increase of peaks *A*, *D*₀, a flattening of peak *D*, and the disappearance of feature *D*₂ are the other relevant changes.

The $\epsilon // a^*$ polarized (solid curve) and $\epsilon // c$ polarized (dotted curve) XANES of the 20 K Mb* photoproduct of MbCO are shown together in Fig. 5, representing the XANES characterization of the low-temperature photoproduct of MbCO.

The difference XANES spectra in the $\epsilon // a^*$ (dotted curve) and $\epsilon // c$ (dashed curve) polarization are shown in Fig. 6. The calculated unpolarized difference spectrum (obtained by a weighted sum of the polarized spectra) is also plotted (solid curve). The figure allows us to compare the present experiment with previous XANES experiments in solution and to reinterpret them (see §4). It is noteworthy that at $E = 7119$ eV the unpolarized difference

spectrum mirrors completely $\epsilon // a^*$ transitions (peak *B*₀), while at $E = 7127$ eV (peak *C*) the unpolarized difference spectrum mirrors the difference $(\epsilon // c) - (\epsilon // a^*)$. Hence at these two energy values the XANES spectrum of the solution sample should contain independent structural information. In contrast, in the energy region 7140–7180 eV the unpolarized difference spectrum contains unresolvable contributions from both the $\epsilon // a^*$ and $\epsilon // c$ polarized transitions.

4. Discussion

As described in §1, the absorption threshold of the spectrum of sperm whale Mb* in solution ($T < 20$ K) is redshifted with respect to MbCO by ~ 1.2 eV, while the spectrum of Mb is known to be redshifted with respect to

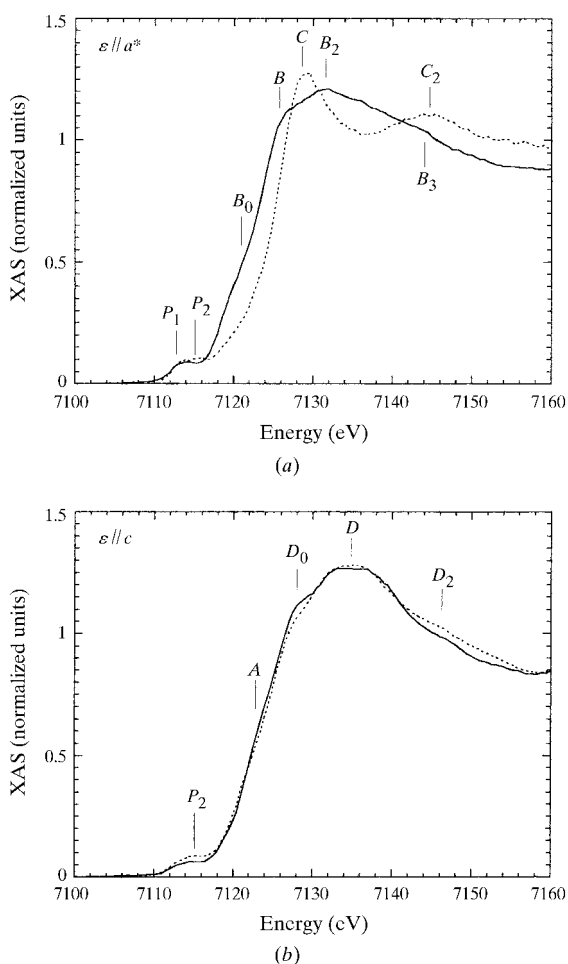


Figure 4
(a) Blow-up of Fig. 3(a), displaying $\epsilon // a^*$ polarized XANES spectra of MbCO and Mb*. Photolysis has a dramatic effect on the spectrum, including a redshift of 2.5 eV of the edge, the disappearance of peaks *C* and *C*₂, and the appearance of new features *B*₀, *B* and *B*₂. (b) Blow-up of Fig. 3(b), displaying $\epsilon // c$ polarized XANES spectra of MbCO and Mb*. Photolysis has a large effect on peak *P*₂, while the changes of peaks *D*₀, *D* and *D*₂ are more limited.

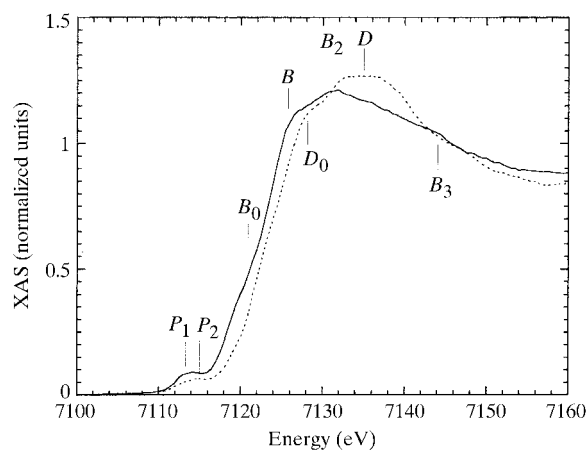


Figure 5
 $\epsilon // a^*$ (solid line) and $\epsilon // c$ (dotted line) polarized XANES spectra of Mb* showing the large XANES dichroism for Mb*. The $\epsilon // a^*$ polarized XANES spectrum probes the distance and orientation of the proximal histidine.

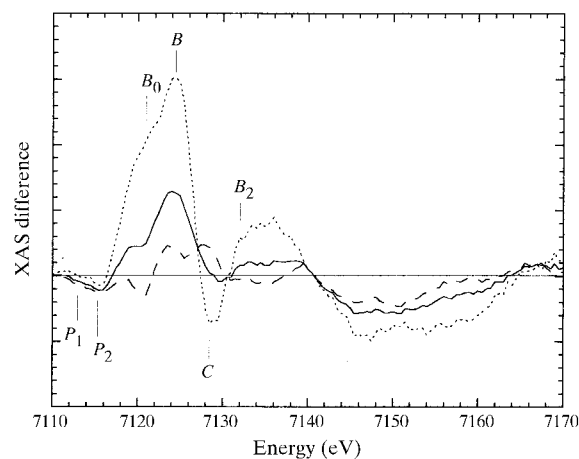


Figure 6
 $\epsilon // a^*$ (dotted curve) and $\epsilon // c$ (dashed curve) polarized XANES difference spectra of Mb*–MbCO. Their weighted sum reproduces the difference spectrum previously reported for a solution sample (Della Longa *et al.*, 1994).

MbCO by ~ 2.5 eV (Chance *et al.*, 1983; Teng *et al.*, 1987; Della Longa *et al.*, 1994). Mb* at 20 K contains a five-coordinated high-spin Fe(II)-heme, like Mb (Roder *et al.*, 1984; Schlichting *et al.*, 1994). Therefore the XANES differences between Mb* and Mb are interpreted in structural terms. It is assumed that the full relaxation at $T = 20$ K of the Fe-heme conformation is not permitted due to the low temperature. According to the Natoli rule (Natoli, 1983) the edge shift going from Mb* to Mb could be related to the lengthening of first-shell distances, *i.e.* lengthening of $d(\text{Fe}-\text{N}_p)$. XANES difference data by XAS in dispersive mode (Della Longa *et al.*, 1994) have already been reported for sperm whale MbCO in solution. By assuming proportionality between the absorption threshold energy of MbCO, Mb* and Mb, and the lengthening of the $d(\text{Fe}-\text{N}_p)$ distance, $d(\text{Fe}-\text{N}_p) = 2.03$ Å for Mb* was determined, a value intermediate between 2.01 Å in MbCO and 2.05 Å in Mb, reported by EXAFS. Della Longa *et al.* (1994) underlined that this value could eventually be altered if a non-linear relationship exists between the spectroscopic observable and the interatomic distance. The polarized data lead us to recognize that the relationship between the energy shift observed in solution and the lengthening of $d(\text{Fe}-\text{N}_p)$ is highly non-linear. In fact, the energy shift of the absorption threshold observed in solution going from

MbCO to Mb* is almost totally due to the electronic relaxation of the empty states with p_z symmetry after breaking of the Fe–CO bond (mirrored in the $\varepsilon // a^*$ XANES, insensitive to the Fe– N_p distance), so that the criterion of proportionality cannot be used to estimate this structural parameter.

Information on the electronic structure of the highest occupied and lowest unoccupied molecular orbital (HOMO–LUMO) of the Fe-heme complex is contained in the pre-edge peaks P_1 and P_2 . The bond with CO includes both σ bonding, $\sigma(\text{CO}) + d_{z^2}(\text{Fe})$ (determining electron donation from the CO σ orbital containing two electrons to the empty d_{z^2} orbital of the low-spin ferrous iron), and π bonding, $\pi^*(\text{CO}) + d_{xz}, d_{yz}(\text{Fe})$ (determining back-donation from the d_{xz}, d_{yz} iron orbitals containing four electrons to the empty π^* orbital of CO).

In the $\varepsilon // a^*$ polarization one expects the pre-edge features to probe electron transitions from the Fe 1s core level to the empty molecular orbitals with z selected symmetry. As already noted, peak P_1 is z -polarized and therefore it probes essentially the d_{z^2} orbital in low-spin ferrous iron, or the Fe–CO σ antibonding orbital [$\sigma(\text{CO}) + d_{z^2}(\text{Fe})$]* in MbCO (the HOMO–LUMO scheme is depicted in Fig. 7a). Because the MbCO \rightarrow Mb* reaction involves a low-spin \rightarrow high-spin transition of the iron, one would expect peak P_1 to decrease in intensity because the electron occupation of the d_{z^2} orbital changes from 0 to 1 (Fig. 7b). At the same time, however, one expects the d – p mixing of the d_{z^2} orbital to increase going from the pseudo-octahedral coordination symmetry in MbCO to the square pyramidal coordination symmetry in Mb*. This latter effect should enhance peak P_1 . Looking at Fig. 4(a), the two opposite effects seem to compensate resulting in a very small decrease of intensity of peak P_1 .

In the $\varepsilon // c$ polarization one expects the pre-edge features to probe transitions from the Fe 1s core level to the empty molecular orbitals with xy selected symmetry, *i.e.* $1s \rightarrow d_{xy}$, $1s \rightarrow \pi^*(\text{porphyrin})$ and the π antibonding orbital $1s \rightarrow [d_{xz}, d_{yz} + \pi^*(\text{CO})]^*$ (HOMO–LUMO scheme in Fig. 8a). The depicted scheme is valid for a linear Fe–C–O bond perpendicular to the heme plane. The CO tilting or bending lowers the overlap between its π^* orbital and the iron d_{xz}, d_{yz} orbitals and enhances the overlap with the π and π^* porphyrin orbitals that combine to form the π bonding and antibonding MO. In the MbCO \rightarrow Mb* reaction the π antibonding orbital disappears. As in the case of the d_{z^2} orbital the electron occupation of the d_{xy} orbital changes from 0 to 1, while the p – d mixing variations imposed by symmetry changes are certainly smaller than for the d_{z^2} orbital. As a result, one expects a lowering of peak P_2 due to decreasing of empty d states of xy symmetry (Fig. 8b).

The energy position of the LUMO orbitals in MbCO and Mb*, as suggested by the measured shape of the pre-edge features of polarized spectra, is shown in Figs. 9(a) and 9(b). An improvement in experimental resolution will be necessary in order to better assign these features. The

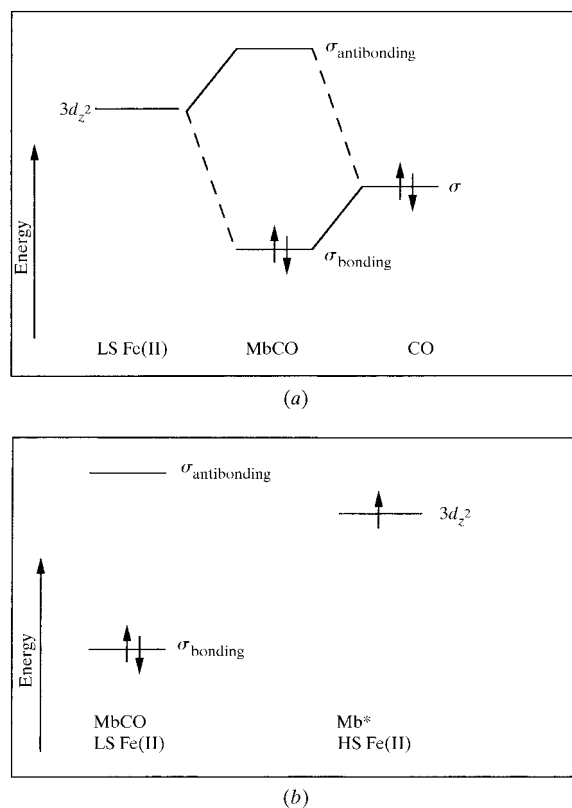
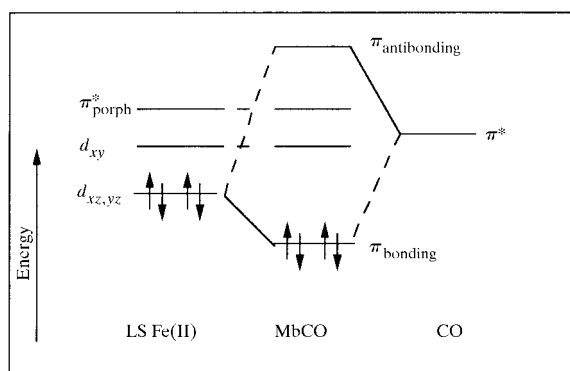


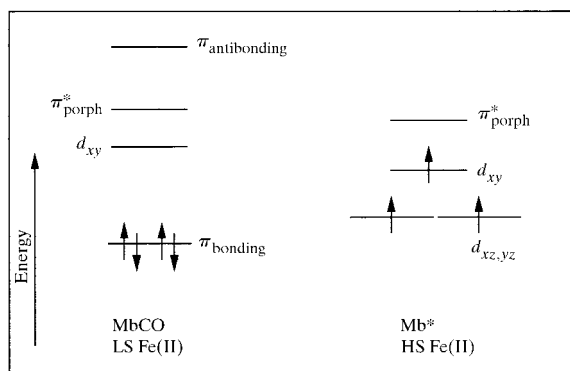
Figure 7
HOMO–LUMO electronic structure concerning $\varepsilon // a^*$ transitions. (a) Formation of σ bonding and antibonding MO between low-spin (LS) Fe(II) and CO in MbCO. (b) Changes in electronic structure going from low-spin Fe(II) MbCO to high-spin (HS) Fe(II) Mb*.

possibility of probing the π antibonding orbital should be important for studying the extent of the iron-to-ligand electron back-donation *via* π bonding. According to the X-ray structure of Kachalova *et al.* (1999) the Fe–CO bond geometry has small deviations from a linear and perpendicular orientation (tilting + bending angle of $\sim 12^\circ$), so that both σ and π bonding can occur in this geometry, in accord with the actual interpretation of the pre-edge features, even if, as suggested by the values of the Fe–C and C–C bond lengths found in the X-ray structure, 1.72 Å and 1.12 Å, respectively, the degree of electron back-donation is small.

As observed in §3 (Fig. 3*b*), the maxima at ~ 7200 and 7270 eV in the EXAFS region of Mb* are redshifted relative to MbCO, suggesting a change in the main frequency of the EXAFS signal, *i.e.* a partial elongation of $d(\text{Fe}-\text{N}_p)$. Because changes at the edge are small (Fig. 4*b*), either XANES is weakly sensitive to this parameter or the Fe– N_p distance variations are very limited. In the latter case, if the residual -1.3 energy shift observed in solution going from Mb* to Mb is due to an increase in the $d(\text{Fe}-\text{N}_p)$ distance, most of the differences should be mirrored in the $\varepsilon // c$ XAS spectrum. The analysis of $\varepsilon // c$ polarized EXAFS will be used to address this point in the future. The small differ-



(a)

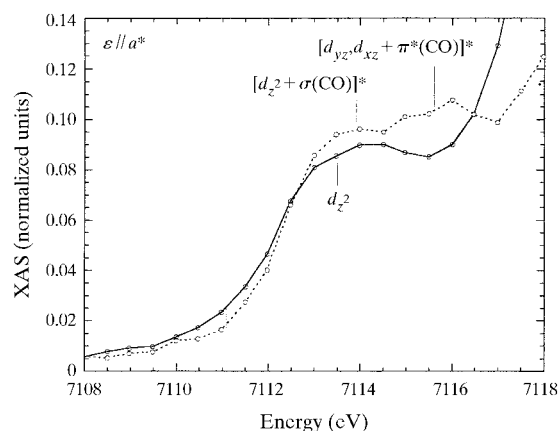


(b)

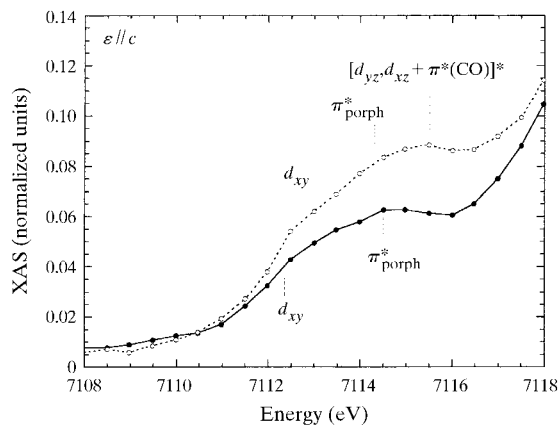
Figure 8

HOMO–LUMO electronic structure concerning $\varepsilon // c$ transitions. (a) Formation of π bonding and antibonding MO between low-spin (LS) Fe(II), porphyrin and CO in MbCO. (b) Changes in electronic structure going from low-spin Fe(II) MbCO to high-spin (HS) Fe(II) Mb*.

ences observed in the $\varepsilon // c$ XANES spectrum going from MbCO to Mb* could be interpreted as spin/structure rearrangement effects on the heme plane. In spite of differences in the iron charge, we find it useful to compare these data with the XANES data reported on the thermal spin transition in Fe(III)Mb⁺OH[−] in solution (Oyanagi *et al.*, 1987; Della Longa, Pin *et al.*, 1998) because only spin/structure effects are present, the ligand always being OH[−]. It is noticeable to see very similar changes over all the XANES range. The absorption threshold is shifted by -0.5 eV or less going from the low-spin to the high-spin derivative of Mb⁺OH[−], and the feature C_2 at ~ 7145 eV (analogous to feature D_2 in Fig. 4*b*) disappears. According to a spin-resolved XANES simulation on Mb⁺OH[−] (Della Longa, Girasole *et al.*, 1998), spin effects and structural effects are both present (*i.e.* unresolvable) in the range 7111–7130 eV, while purely structural effects dominate above 7130 eV, including peak C_2 in low-spin Mb⁺OH[−]. The influence of the Fe spin state on the XANES simulations is due to changes in the local exchange-correlation potential term V_{ex} which, for electronic states with σ -type



(a)



(b)

Figure 9

Tentative assignment of electronic levels within the pre-edge features P_1 and P_2 of experimental spectra, as indicated in the figures. Improvement in energy resolution will be necessary for a definitive assignment of the features.

spin, can be written as $V_{\text{ex},\sigma}(r) = -6\alpha[(3/4)\rho_{\sigma}(r)]^{1/3}$. In this expression $\rho_{\sigma}(r)$ is a total local charge density of electrons with spin σ , and α is the exchange constant. According to these simulations a very small (-0.5 eV) energy shift of the absorption threshold can arise as a spin effect. The same analogy can be extended to feature D_2 . Its disappearance on going from MbCO to Mb* should reflect symmetry changes of the $\text{Fe}(\text{N}_p)_4$ coordination going from the low-spin to the high-spin derivative, consequent to a small displacement of the Fe atom along the heme normal.

The ligand effect is also strong in the LFIR region (7150–7250 eV) of the $\varepsilon // a^*$ spectrum; this result does not agree with the hypothesis that changes in this region are due simply to reorientation of pyrrolic rings, and with the consequent proposed measure of the Fe displacement in both six-coordinated and five-coordinated heme derivatives in solution in the same calibration curve (Miller & Chance, 1995).

In this experiment we did not investigate the effect of light on the Fe-heme structure. A more accurate study using monochromatic light allowing the number of photons absorbed per molecule to be quantified would assess the possible effects on the Fe–His bond (Ahmed *et al.*, 1991), and would provide detailed information about tunnelling effects (Ober *et al.*, 1997) in the recombination process.

In summary, the overall XANES results in Mb* seem consistent with the X-ray data of Teng *et al.* (1997), reporting a small relaxation of the Fe-heme ($\sim 30\%$), corresponding to an Fe-heme displacement of ~ 0.1 Å. As mentioned above, the energy shift of the absorption edge going from MbCO to Mb* (~ 1.2 eV) is almost totally due to ligand dissociation. However, an accurate study of the thermally and light-induced changes in the polarized XAS, and the comparison between polarized XAS of ligated and unligated Fe-heme states, would lead to the measure of other parameters probing selectively the heme relaxation. If heme relaxation and ligand rebinding are two distinct processes (Franzen & Boxer, 1997), polarized XAS promises to be powerful in allowing the observation, in the same experiment, of these complementary aspects of a protein dynamic event. In such a way the present experiment opens the way to a systematic EXAFS investigation on the time- (over long times), temperature- (4–60 K), and illumination-dependence of single parameters like $d(\text{Fe}-\text{N}_p)$, $d(\text{Fe}-\text{N}_e)$ in the cryogenic unligated photoproduct. We have already verified the feasibility of the experiment by collecting preliminary polarized EXAFS spectra in the range $2-13$ Å $^{-1}$. Polarized EXAFS could be applied to check the controversial hypothesis of a proximal control of the rebinding barrier, relying on changes in position of the iron-histidine complex of the order of 0.1 Å or less. A careful analysis of the first Fourier peak in the polarized EXAFS spectra should give precise values of the first-shell distances around the Fe atom to 0.02 Å. However, a problem remains concerning data analysis. In our opinion the definitely convincing EXAFS analysis applied to such a dynamic problem should fit simultaneously the angular-

resolved spectra, including (i) a correct curved-wave EXAFS dichroism theory, (ii) multiple scattering contributions, (iii) search for multiple excitation edges. Even though any of these correction terms are separately included in the available software packages, we are not aware of a package including all of them.

Thanks are due to Professor M. Bolognesi for supplying the crystal samples and for helpful discussions. The authors are indebted to Professor J. C. Fontecilla, Professor M. Frey of the Institute de Biologie Structurale (IBS) for the kind hospitality received in the Institute. The authors also thank the staff of EMBL Grenoble Outstation Laboratory for hospitality and assistance. Finally, special thanks are due to Emma Wilson for her kindness and patience. This work was supported by Grants of INFM, Italy, and by the EC's TMR programme.

References

- Ahmed, A. M., Campbell, B. F., Caruso, D., Chance, M. R., Chavez, M. D., Courtney, S. H., Friedman, J. M., Iben, I. E. T., Ondrias, M. R. & Yang, M. (1991). *Chem. Phys.* **158**, 329–351.
- Alben, J. O., Beece, D., Bowne, S. F., Eisenstein, L., Frauenfelder, H., Good, D., Marden, M. C., Moh, P. P., Reinisch, L., Reynolds, A. H. & Yue, K. T. (1980). *Phys. Rev. Lett.* **44**, 1157–1160.
- Austin, R. H., Benson, K. W., Eisenstein, L., Frauenfelder, H. & Gunsalus, I. C. (1975). *Biochemistry*, **14**, 5355–5373.
- Bianconi, A., Congiu Castellano, A., Durham, P. J., Hasnain, S. S. & Phillips, S. (1985). *Nature (London)*, **318**, 685–687.
- Cartier, C., Momenteau, M., Dartyge, E., Fontaine, A., Tourillon, G., Bianconi, A. & Verdaguer, M. (1992). *Biochem. Biophys. Acta*, **1119**, 169–174.
- Case, D. A. & Karplus, M. (1979). *J. Mol. Biol.* **132**, 343–368.
- Chance, B., Fischetti, R. & Powers, L. (1983). *Biochemistry*, **22**, 3820–3829.
- Chance, M. R., Miller, L. M., Fischetti, R. F., Scheuring, E., Huang, W.-X., Sclavi, B., Hai, Y. & Sullivan, M. (1995). *Biochemistry*, **35**, 9014–9023.
- Chance, M. R., Parkhurst, L. J., Powers, L. & Chance, B. (1986). *J. Biol. Chem.* **261**, 5689–5692.
- Della Longa, S., Ascone, I., Fontaine, A., Congiu Castellano, A. & Bianconi, A. (1994). *Eur. Biophys. J.* **23**, 361–368.
- Della Longa, S., Girasole, M., Congiu Castellano, A., Bianconi, A., Kovtun, A. P. & Soldatov, A. V. (1998). *Eur. Biophys. J.* **27**, 541–548.
- Della Longa, S., Pin, S., Cortes, R., Soldatov, A. V. & Alpert, B. (1998). *Biophys. J.* **75**, 3154–3162.
- Eisenberger, P., Shulman, R. G., Kincaid, B. M., Brown, G. S. & Ogawa, S. (1978). *Nature (London)*, **274**, 30–34.
- Elber, R. & Karplus, M. (1987). *Science*, **235**, 318–321.
- Franzen, S., Bohn, B., Poyart, C. & Martin, J. L. (1995). *Biochemistry*, **34**, 1224–1237.
- Franzen, S. & Boxer, S. G. (1997). *J. Biol. Chem.* **272**, 9655–9660.
- Iizuka, T., Yamamoto, H., Kotani, M. & Yonetani, T. (1974). *Biochim. Biophys. Acta*, **371**, 126–139.
- Kachalova, G. S., Popov, A. N. & Bartunik, H. D. (1999). *Science*, **284**, 473–476.
- Kuriyan, J., Wilz, S., Karplus, M. & Petsko, G. A. (1986). *J. Mol. Biol.* **192**, 133–154.

- Lambright, D. G., Balasubramanian, S. & Boxer, S. G. (1991). *Chem. Phys.* **158**, 249–260.
- Lim, M., Jackson, T. A. & Anfinsen, P. A. (1997). *Nat. Struct. Biol.* **4**, 209–214.
- Miller, L. M. & Chance, M. R. (1995). *Biochemistry*, **34**, 10170–10179.
- Natoli, C. R. (1983). *EXAFS and Near Edge Structure*, edited by A. Bianconi, L. Incoccia & S. Stipcich, pp. 43–56. Berlin: Springer.
- Nienhaus, G. U., Mourant, J. R., Chu, K. & Frauenfelder, H. (1994). *Biochemistry*, **33**, 13413–13430.
- Ober, C., Burkhardt, M., Winkler, H., Trautwein, A. X., Zharikov A. A., Fisher, S. F. & Parak, F. (1997). *Eur. Biophys. J.* **26**, 227–237.
- Oyanagi, H., Iizuka, T., Matsushita, T., Saigo, S., Makino, R., Ishimura, Y. & Ishiguro, T. (1987). *J. Phys. Soc. Jpn*, **56**, 3381–3388.
- Phillips, G. N. Jr (1990). *Biophys. J.* **57**, 381–383.
- Pin, S., Alpert, B., Congiu Castellano, A., Della Longa, S. & Bianconi, A. (1994). *Methods Enzymol.* **232**, 266–292.
- Powers, L., Chance, B., Chance, M., Campbell, B., Khalid, J., Kumar, C., Naqui, A., Reddy, K. S. & Zhou, Y. (1987). *Biochemistry*, **26**, 4785–4796.
- Powers, L., Sessler, J. L., Woolery, G. L. & Chance, B. (1984). *Biochemistry*, **23**, 5519–5523.
- Quillin, M. L., Arduini, R. M., Olson, J. S. & Phillips, G. N. Jr (1993). *J. Mol. Biol.* **234**, 140–155.
- Roder, H., Berendzen, J., Bowne, S. F., Frauenfelder, H., Sauke, T. B., Shyamsunder, E. & Weissman, B. (1984). *Proc. Natl Acad. Sci. USA*, **81**, 2359–2363.
- Sassaroli, M. & Rousseau, D. L. (1986). *J. Biol. Chem.* **261**, 16292–16294.
- Schlichting, I., Berendzen, J., Phillips, G. N. Jr & Sweet, R. M. (1994). *Nature (London)*, **371**, 808–812.
- Scott, E. E. & Gibson, Q. H. (1997). *Biochemistry*, **36**, 11909–11917.
- Srajer, V., Teng, T. Y., Ursby, T., Pradervand, C., Ren, Z., Adachi, S. I., Schildkamp, W., Bourgeois, D., Wulff, M. & Moffat, K. (1996). *Science*, **274**, 1726–1729.
- Steinbach, P. J., Ansari, A., Berendzen, J., Braunstein, D., Chu, K., Cowen, B. R., Ehrenstein, D., Frauenfelder, H., Johnson, J. B., Lamb, D. C., Luck, S., Mourant, J. R., Nienhaus, G. U., Ormos, P., Philipp, R., Xie, A. & Young, R. D. (1991). *Biochemistry*, **30**, 3988–4001.
- Teng, T.-Y., Huang, H. W. & Olah, G. A. (1987). *Biochemistry*, **26**, 8066–8072.
- Teng, T.-Y., Srajer, V. & Moffat, K. (1997). *Biochemistry*, **36**, 12087–12100.
- Vitkup, D., Petsko, G. A. & Karplus, M. (1997). *Nat. Struct. Biol.* **4**, 202–208.